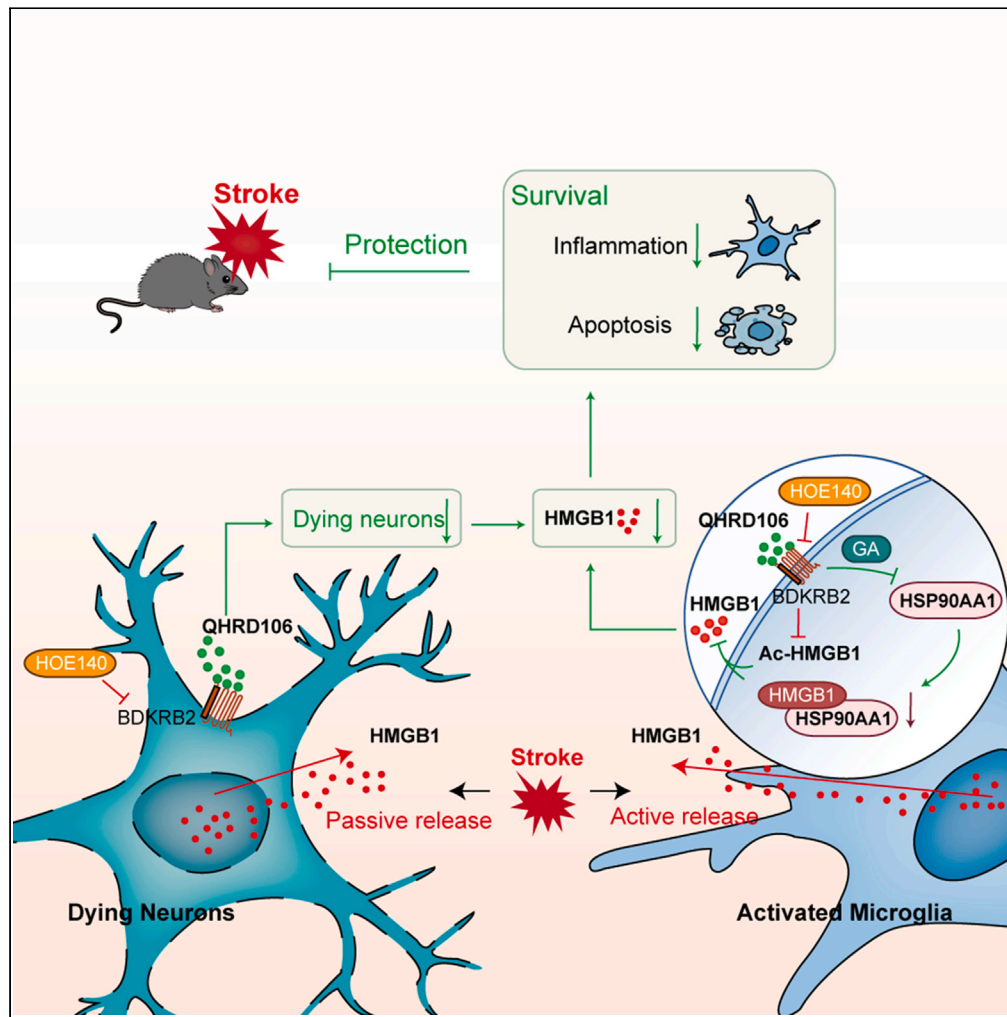# iScience

Article

QHRD106 ameliorates ischemic stroke injury as a long-acting tissue kallikrein preparation

Si-Yi Xu, Jun-Qiu
Jia, Min Sun, ..., Lei
Ye, Xiang Cao,
Yun Xu

xiangcao1988@163.com (X.C.)
xuyun20042001@aliyun.com
(Y.X.)

Highlights

QHRD106 is a long-acting
intramuscular tissue
kallikrein injection

QHRD106 attenuates
ischemic stroke injury
through B2R instead of
B1R

QHRD106 reduces
HMGB1 release by
neurons and microglial
cells after ischemic stroke

iScience

Article

QHRD106 ameliorates ischemic stroke injury as a long-acting tissue kallikrein preparation

Si-Yi Xu,[1,2,6] Jun-Qiu Jia,[2,6] Min Sun,[2] Xin-Yu Bao,[2,3,4,5] Sheng-Nan Xia,[2,3,4,5] Shu Shu,[2,3,4,5] Pin-yi Liu,[2,3,4,5] Sen-lin Ji,[2,3,4,5] Lei Ye,[2] Xiang Cao,[1,2,3,4,5,*] and Yun Xu[1,2,3,4,5,7,*]

SUMMARY

Ischemic stroke is the second leading cause of death worldwide, and there are limited effective treatment strategies. QHRD106, a polyethyleneglycol (PEG)-modified long-acting tissue kallikrein preparation, has not been reported previously. In this study, we aimed to investigate the therapeutic effect of QHRD106 in ischemic stroke and its possible mechanism. We found that QHRD106 treatment alleviated brain injury after stroke via bradykinin (BK) receptor B2 (B2R) instead of BK receptor B1 (B1R). Mechanistically, QHRD106 reduced high-mobility group box 1 (HMGB1)-induced apoptosis and inflammation after ischemic stroke in vivo and in vitro. Moreover, we confirmed that QHRD106 reduced the level of acetylated HMGB1 and reduced the binding between heat shock protein 90 alpha family class A member 1 (HSP90AA1) and HMGB1, thus inhibiting the translocation and release of HMGB1. In summary, these findings indicate that QHRD106 treatment has therapeutic potential for cerebral ischemic stroke.

INTRODUCTION

Stroke is the second leading cause of death worldwide and is usually classified as ischemic or hemorrhagic stroke. Statistically, almost 87% of stroke cases are ischemic stroke.[1,2] Poststroke treatment usually falls into two main categories: reperfusion therapy and neuroprotection therapy. Although either mechanically or pharmacologically removing clots and restoring brain blood supply are essential and effective for patients with acute ischemic stroke, only a tiny minority of patients benefit from these treatments because of the narrow time window and the increased risk of complications.[3,4] Therefore, effective poststroke neuroprotective treatments are urgently needed to improve the prognosis of stroke patients.

The penumbra surrounds the core of the ischemic area, accounting for half of the total lesion volume. Although neurons in the penumbra are electrophysiologically silenced and functionally depressed, these cells are still viable at early time points.[5,6] Thus, saving ischemic penumbral tissue is of great significance as smaller infarcts correlate with better neurological outcomes.[7,8] Additionally, neuroinflammation has been recognized as a key factor in the onset and progression of stroke. Microglia, the resident immune cells in the brain, are activated within minutes and remain activated for days to weeks after stroke. These microglia secrete a large number of inflammation-related cytokines, such as tumor necrosis factor (TNF), inducible nitric oxide synthase (iNOS), interleukins (ILs), and high-mobility group box 1 (HMGB1), causing inflammatory responses and aggravating neuronal death.[9–12] Emerging evidence has shown that inhibition of microglia-mediated inflammation in the acute phase after stroke can inhibit neuronal apoptosis and improve prognosis.[13,14]

HMGB1, a nonhistone nuclear protein, performs different functions according to its subcellular location. In the nucleus, it acts as a DNA chaperone and plays a role in the replication and repair of DNA, maintaining the structure and function of chromosomes. However, after ischemia, HMGB1 is actively secreted by immune cells or passively released by necrotic cells as a damage-associated molecular pattern (DAMP) molecule that directly or indirectly mediates inflammatory responses and apoptosis.[15–19] In ischemic animal models, HMGB1 translocations in neurons around cortical infarction appear shortly after reperfusion.[20–22] Increasing evidence suggests that HMGB1 levels in the cerebrospinal fluid (CSF) and serum increase rapidly 3 h after stroke and generate two peaks: one on the 1st day and one on the 7th day after stroke.[20,23] The increases last for at least 2 weeks in animal models following ischemia but even longer in ischemic stroke patients.[24,25] Extracellular HMGB1 activated the mitogen-activated protein kinase (MAPK) and

[1]Department of Neurology, Nanjing Drum Tower Hospital Clinical College of Jiangsu University, Nanjing, Jiangsu 210008, P.R. China

[2]Department of Neurology, Nanjing Drum Tower Hospital, Affiliated Hospital of Medical School and State Key Laboratory of Pharmaceutical Biotechnology, Institute of Translational Medicine for Brain Critical Diseases, Nanjing University, Nanjing, Jiangsu 210008, P.R. China

[3]Jiangsu Key Laboratory for Molecular Medicine, Medical School of Nanjing University, Nanjing, Jiangsu 210008, P.R. China

[4]Jiangsu Provincial Key Discipline of Neurology, Nanjing, Jiangsu 210008, P.R. China

[5]Nanjing Neurology Medical Center, Nanjing, Jiangsu 210008, P.R. China

[6]These authors contributed equally

[7]Lead contact

*Correspondence: xiangcao1988@163.com (X.C.), xuyun20042001@aliyun.com (Y.X.)

https://doi.org/10.1016/j.isci.2023.107268

nuclear factor κB (NF-κB) signaling pathways and contributed to the inflammatory response.[26] Pharmacological inhibition of HMGB1 or its downstream pathway after ischemia protects the brain against ischemic hypoxia injury.[27–29] The mechanism of HMGB1 translocation is very complicated. Many studies have indicated that hyperacetylation of HMGB1 affects its DNA binding activity and induces its translocation and secretion.[16,30,31] However, additional mechanisms affecting the nucleocytoplasmic translocation and secretion of HMGB1 remain to be explored.

The kallikrein-kinin system (KKS) is a complex multienzyme system *in vivo* that plays an important role in vascular permeability, inflammation, thrombosis, coagulation, and other processes. Its main components are kininogen, kallikrein, and bradykinin (BK). Kallikrein includes tissue kallikrein (TK) and plasma kallikrein (PK), which act on the kininogen to produce BK. As the main effector molecule of the KKS, BK plays its biological role by binding with two types of G-protein-coupled receptors: B1R and B2R.[32] A series of studies have proven that TK treatment is beneficial after ischemic stroke. TK alleviates oxidative stress, neuroinflammation, and apoptosis and promotes neuronal survival after ischemia.[33–35] Additionally, TK can reduce lipopolysaccharide (LPS)-induced neuroinflammation and oxidative stress in BV-2 cells.[36] Moreover, it has been reported that TK enhances B2R-mediated MEK1/2/ERK1/2 and AMPK/TSC2/mTOR signaling under oxygen-glucose deprivation/reoxygenation (OGD/R) stress in human SH-SY5Y neuronal cells, inducing protective autophagy.[37] QHRD106 (molecular formula: $C_{1174}H_{1766}N_{306}O_{356}S_{14}$ + $(C_2H_4O)_n$; molecular weight: 112.5; chemical name: (3-(α-methylpoly(oxyethylene)oxy)propanamido)$_8$tissue kallikrein) is a PEG-modified long-acting TK preparation that has not been reported previously. Given the efficacy of TK, we hypothesized that QHRD106 might also exert protective effects against ischemic stroke.

In this study, we aimed to investigate the therapeutic effects of QHRD106 treatment on ischemic stroke and to identify the underlying mechanisms. We found that QHRD106 ameliorated mouse neurological deficits, decreased HMGB1 cytoplasmic translocation and secretion in neurons and microglial cells *in vivo* and *in vitro*, and subsequently alleviated HMGB1-induced neuroinflammation and apoptosis after ischemic stroke. In addition, we discovered that QHRD106 not only inhibited the acetylation of HMGB1 but also decreased the binding between heat shock protein 90 alpha family class A member 1 (HSP90AA1) and HMGB1, thus decreasing the translocation and secretion of HMGB1 in microglia.

RESULTS

QHRD106 protected against infarction and neurological deficits after stroke via BK B2 receptor (B2R)

QHRD106 is a PEG-modified, long-acting preparation of TK. And its structural formula is provided in Figure S1A. First, a middle cerebral artery occlusion (MCAO) mouse model was established to replicate ischemic stroke *in vivo*. Laser speckle contrast imaging (LSCI) showed that cerebral blood flow (CBF) was reduced to nearly 39.8% ± 2.8% after MCAO and restored to 84.7% ± 2.8% after reperfusion and injection of saline or QHRD106 for 1 h, and QHRD106 injection did not change the ultimate CBF (Figures S1B and S1C). These results implied that the mouse MCAO model was successfully established and that QHRD106 injection had no effect on CBF during the process. Next, we investigated the effective dose of QHRD106 in mouse MCAO models. The mice were randomly divided, and three different doses of QHRD106 (100, 200, and 400 IU/kg) were used. Ischemia-induced neurological deficits were measured by the rotarod test, forepaw grip strength measurement, and modified neurological severity score (mNSS) assessment (Figures S1D–S1F). QHRD106-400 IU/kg-treated mice persisted longer in the rotarod test and showed higher forepaw grip strength within 3 days of stroke than mice in the saline group. In addition, the mNSS of QHRD106-400 IU/kg-treated mice was lower, which indicated better neurological function after stroke. These data indicated that treatment with QHRD106-400 IU/kg significantly improved neurological deficits after stroke. Therefore, the dose of 400 IU/kg was selected for our following experiment.

To identify the type of receptors through which QHRD106 exerts its protective effect, we combined QHRD106 with R-715, a potent and selective B1R antagonist, or with HOE-140, a potent and specific antagonist of B2R. As shown in Figures S1G–S1I, the results of the rotarod test, forepaw grip strength measurement, and mNSS indicated that the addition of R-715 did not reduce the protective effect of QHRD106. As shown in Figures 1B and 1C, HOE-140 reversed the protective effect of QHRD106 on brain infarction size on days 3 and 7 after stroke (p < 0.05). Similarly, HOE-140 reversed the protective effects of QHRD106 on mouse with neurological deficits, as measured by the rotarod test, forepaw grip strength measurement, and mNSS scoring (Figures 1D–1F). These results confirmed that QHRD106 could decrease the infarct
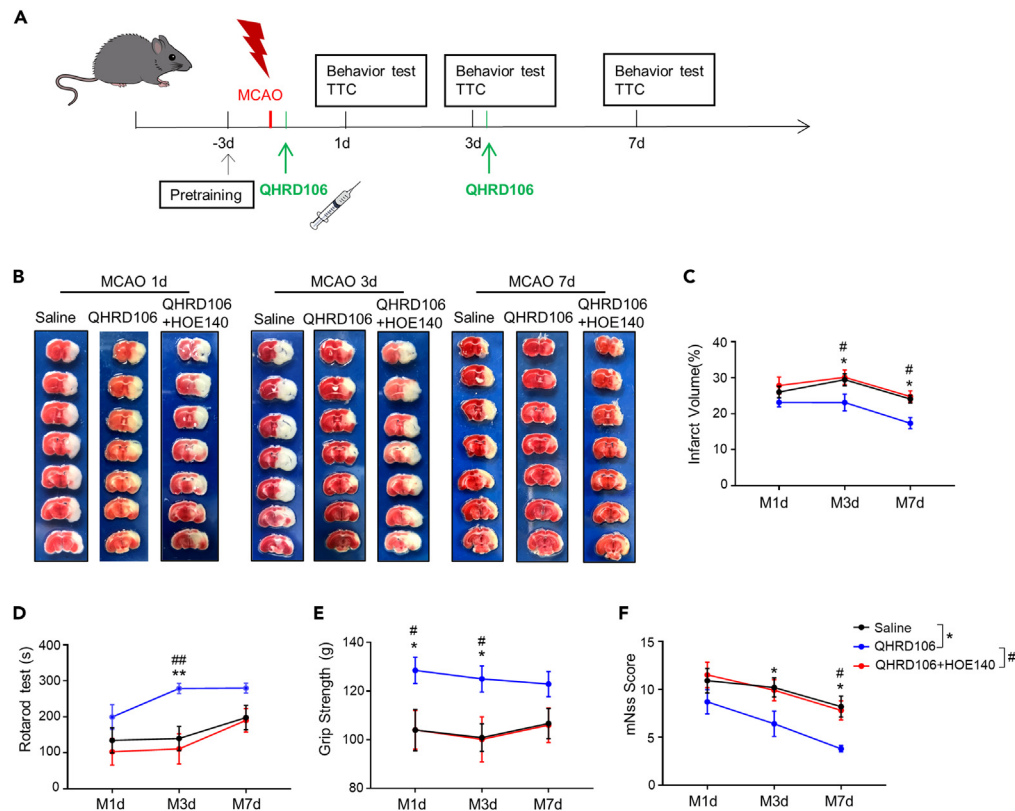
Figure 1. QHRD106 protected against infarction and neurological deficits via B2R after MCAO at different time points

(A) Timeline of the experimental procedure.

(B) Representative brain sections stained with TTC in MCAO model mice 1, 3, and 7 days poststroke.

(C) Infarct volume (n = 10 mice per group).

(D) Rotarod test results (n = 10 mice per group).

(E) Grip strength (n = 10 mice per group).

(F) mNSS scores (n = 10 mice per group).

All data are presented as the mean ± SEM. Statistical analyses were performed by two-way ANOVA followed by Tukey's post hoc test. *$p < 0.05$, **$p < 0.01$ vs. the saline group; #$p < 0.05$, ##$p < 0.01$ vs. the QHRD106 group.

volume and improve the neurological functions of mice after ischemic stroke and that the protective effect may be mediated by B2R instead of B1R.

QHRD106 protected against stroke-induced apoptosis and neuroinflammation via B2R

On the basis of previous behavioral test results, we chose the third day after MCAO as the time point for subsequent *in vivo* research. Apoptosis and inflammation are two major pathophysiological events following ischemia/reperfusion that are closely related to the prognosis of stroke.[38] To assess the effects of QHRD106 treatment on neuronal apoptosis after stroke, TUNEL staining was used (Figures 2A and 2B). The percentage of TUNEL-positive neurons increased dramatically in the peripheral infarct area of the saline group compared to the sham group three days after MCAO. However, the administration of QHRD106 greatly decreased the percentage of apoptotic neurons ($p < 0.01$), and additional HOE-140 treatment diminished this protection ($p < 0.01$). Classic apoptosis-regulating proteins, Bax and Bcl-2, were examined by western blot analysis (Figures 2C and 2D). As expected, MCAO elevated the Bax/Bcl-2 ratio compared with that in the sham group. In addition, the ratio was significantly decreased after QHRD106 injection, and this change was diminished by HOE-140 treatment ($p < 0.05$). These data showed that QHRD106 treatment plays a key role in decreasing cell apoptosis after cerebral ischemia/reperfusion and that this protective effect may be mediated by B2R. In the following experiments, we measured the protein levels of some inflammation-related cytokines in the peri-infarct penumbra three days after MCAO (Figures 2E–2H). Western blot results showed that the expression of iNOS ($p < 0.05$), MCP-1
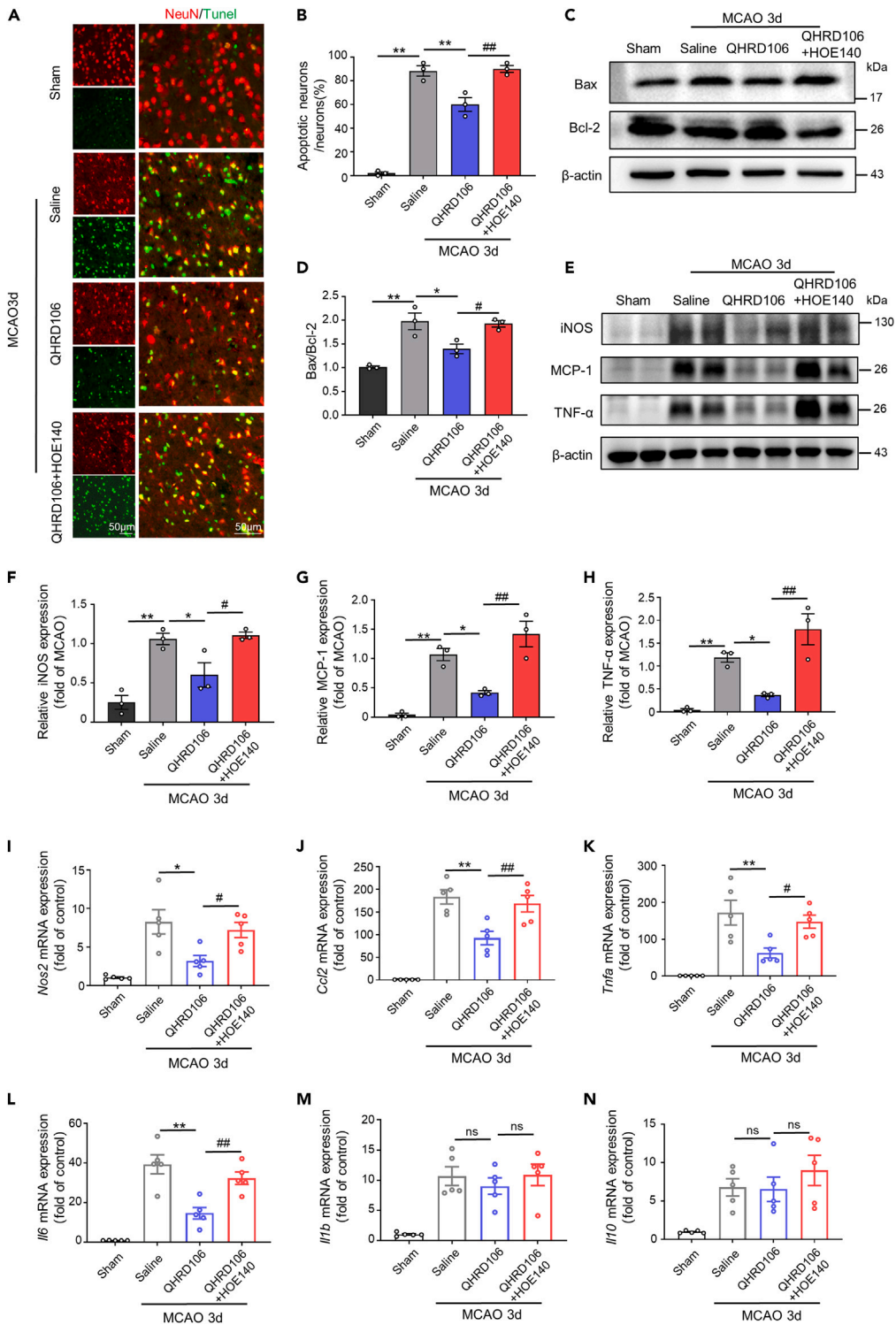
Figure 2. QHRD106 protected against apoptosis and neuroinflammation via B2R during stroke

(A) Representative dual-immunofluorescence staining of NeuN (red)/TUNEL (green).

(B) The percentage of NeuN+TUNEL+ cells among all NeuN+ cells in the peri-infarct brain regions (n = 3/group; one-way ANOVA and Tukey's post hoc test.

(C) Representative western blot images of Bax, Bcl-2, and β-actin expression in the ischemic penumbras of mice 3 days poststroke.

Figure 2. Continued

(D) Quantification of Bax/Bcl-2.

(E–H) Representative western blots and quantitative analysis of the proinflammatory cytokine levels of iNOS, MCP-1, and TNF-α in the ischemic penumbras of mice 3 days poststroke.

(I–N) The mRNA levels of *Nos2, Ccl2, Tnfa, Il6, Il1b,* and *Il10* in the ischemic penumbras of MCAO mice 3 days poststroke were detected via quantitative real-time PCR.

All data are presented as the mean ± SEM. Statistical analyses were performed by one-way ANOVA followed by Tukey's post hoc test. *p < 0.05, **p < 0.01 vs. the saline group; #p < 0.05, ##p < 0.01 vs. the QHRD106 group; "ns" indicates no significance (p > 0.05).

(p < 0.01), and TNF-α (p < 0.01) was significantly decreased by QHRD106 treatment compared to that in the saline group. Furthermore, as shown in Figures 2I–2L, the mRNA levels of proinflammatory factors (*Nos2, Ccl2, Tnfa, Il6*) were increased after MCAO but significantly decreased after QHRD106 injection. However, HOE-140 reversed the anti-inflammatory effects of QHRD106 on the mRNA and protein levels of inflammatory cytokines. Notably, QHRD106 had no significant effects on the mRNA level of the proinflammatory factor *Il1b* or the anti-inflammatory factor *Il10* (Figures 2M and 2N). As a result, we concluded that QHRD106 may decrease apoptosis and neuroinflammation after stroke via B2R.

QHRD106 protected against stroke via B2R by decreasing HMGB1 translocation and secretion

To identify the possible mechanism by which QHRD106 protected mice against ischemia/reperfusion insult, we performed proteomics experiments on the brains of mice in the saline group and the QHRD106 group three days after stroke. Based on the fold change (≥1.2) and p value (≤0.05), 61 differentially expressed proteins (DEPs) were identified. Compared to mice in the MCAO group, those in the QHRD106 group had 11 upregulated and 50 downregulated DEPs. We noticed that these DEPs were mostly related to apoptotic processes (Gulp1, Hmgb1, Ahsg, etc.), the inflammatory response (Apoa1, Orm1, Rbp4, Hmgb1, etc.), and immune system processes (Gc, Myo1e, Anxa3, Hmgb1, etc.) (Figure 3A). To investigate the possible mechanism further, we conducted kyoto encyclopedia of genes and genomes (KEGG) and gene ontology (GO) analyses on the DEPs. KEGG pathway analysis indicated the possible pathways altered by QHRD106 treatment after stroke. GO analysis of DEPs was further employed to characterize their biological functions in three categories: molecular function, cellular component, and biological process. These results indicated that QHRD106 may protect against ischemic stroke by attenuating apoptosis and inflammation (Figures 3B and 3C).

HMGB1 acts as a DAMP after it is translocated and released, aggravating further inflammation and apoptosis after stroke. After obtaining the proteomics results, we next investigated whether QHRD106 exerts its protective function after stroke by affecting HMGB1. Posttranslational modifications such as acetylation play important roles in the nucleocytoplasmic translocation and secretion of HMGB1. We found that the acetylation level of HMGB1 dramatically increased after stroke (p < 0.01) and that QHRD106 significantly impaired the acetylation of HMGB1 (p < 0.05) (Figures S2A and S2B). Then, proteins of the cell nucleus and cytoplasm from lesioned cortices were extracted, and subsequent western blot analysis was used to detect HMGB1 translocation (Figures 3D–3F). The results showed that HMGB1 levels in the cytosol significantly increased after the MCAO procedure (p < 0.05) and that QHRD106 treatment effectively decreased HMGB1 levels in the cytoplasm (p < 0.05), indicating that QHRD106 decreased the cytoplasmic translocation of HMGB1 after stroke. On the other hand, HOE-140 attenuated the effects of QHRD106 on HMGB1 translocation (p < 0.05). There was no significant difference in nuclear HMGB1 expression among the four groups. Serum HMGB1 levels are closely related to the severity and prognosis of stroke.[39,40] Thus, ELISA was used to measure serum HMGB1 levels, reflecting the degree of HMGB1 release (Figure 3G). The timeline was extended to 7 days after stroke to observe the level of HMGB1 release. The results showed that QHRD106 dramatically attenuated the increase in the level of HMGB1 in serum after stroke (p < 0.01). Additional HOE-140 diminished the effect of QHRD106 in decreasing serum HMGB1 7 days after stroke (p < 0.01). These *in vivo* results indicated that QHRD106 may protect against neurological deficits after stroke via B2R by decreasing HMGB1 translocation and secretion.

QHRD106 decreased neuronal and microglial HMGB1 translocation *in vivo* via B2R and inhibited overactivation of microglia

HMGB1 can be passively released by necrotic neurons or actively secreted by microglia in the brain.[23] Thus, double immunofluorescence staining was used to reveal the location of HMGB1 in neurons (NeuN[+]) and
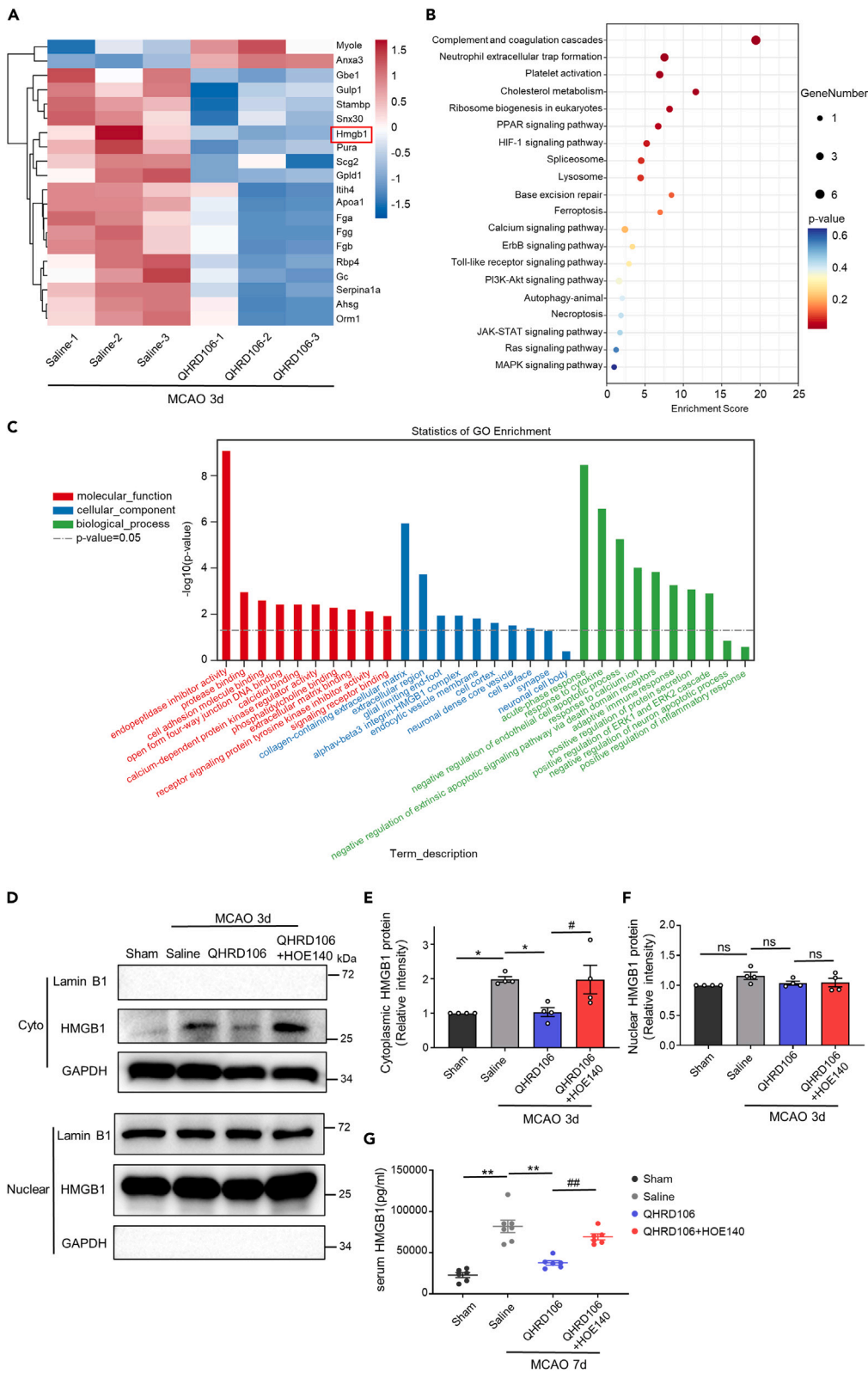
Figure 3. QHRD106 protected against stroke via B2R by decreasing HMGB1 translocation and secretion

(A–C) The brains of mice in the saline group and QHRD106 group 3 days after MCAO were analyzed in a proteomics experiment. (A) Heatmap of DEPs between the saline group and the QHRD106 group. (B) KEGG pathway analysis of DEPs. (C) GO analysis of the DEPs, including three categories: biological processes, cellular components, and molecular functions.

(D–F) The nucleocytoplasmic translocation of HMGB1 was evaluated by western blot analysis. GAPDH and Lamin B1 were used as cytoplasmic and nuclear loading controls, respectively.

(G) Serum HMGB1 levels were evaluated by ELISA in mice 7 days poststroke.

All data are presented as the mean ± SEM. Statistical analyses were performed by one-way ANOVA followed by Tukey's post hoc test. *$p < 0.05$, **$p < 0.01$ vs. the saline group; #$p < 0.05$, ##$p < 0.01$ vs. the QHRD106 group, "ns" indicates no significance ($p > 0.05$).

microglia (Iba-1^{+}) under different circumstances. HMGB1-positive staining only in the nucleus indicated that HMGB1 had not been translocated. Once HMGB1 was present in the cytoplasm or extracellular space, we assumed that HMGB1 translocation had occurred.

As shown in Figures 4A–4D, HMGB1 only localized in the nucleus in the sham group. The translocation of HMGB1 from the nucleus to the cytosol and extracellular space was obvious in neurons one and three days after MCAO ($p < 0.01$). However, QHRD106 treatment significantly inhibited the translocation of HMGB1 compared with that in the saline group. Additional HOE-140 diminished the effect of QHRD106 in decreasing HMGB1 translocation in neurons after stroke ($p < 0.01$). We also observed the translocation conditions of HMGB1 in microglial cells after MCAO. As shown in Figures 4E–4G, HMGB1 translocation in microglia did not occur one day after MCAO but was obvious on the third day after MCAO ($p < 0.01$). Similarly, QHRD106 treatment significantly inhibited the translocation of HMGB1 on the third day after MCAO ($p < 0.01$). Additional HOE-140 decreased the effect of QHRD106 on microglial HMGB1 translocation after stroke ($p < 0.05$). These results showed that QHRD106 can reduce both HMGB1 passive release by necrotic neurons and active release by microglia after MCAO and that these protective effects might be achieved via B2R.

After cerebral ischemia, excessively activated microglia release large amounts of HMGB1 into the extracellular space. Microglia in the normal state display a ramified morphology, but microglia acquire a less ramified morphology, shorter process length, and higher fluorescence intensity after ischemia.[41–43] Thus, automated microglial morphological analysis and fluorescence intensity analysis were conducted with ImageJ to determine the activation level of microglia. As shown in Figures 4H–4J, the branching complexity and process length of microglia in the saline group were attenuated one or three days after stroke compared with those in the sham group, suggesting that microglia were activated ($p < 0.01$). QHRD106 treatment decreased microglial activation compared with that in the saline group. Additional HOE-140 nonsignificantly decreased the effect of QHRD106 on microglial morphology. However, differences in microglial morphology one day after stroke among the saline group, QHRD106 group, and QHRD106+HOE-140 group were not obvious, although there seemed to be a trend. As shown in Figure 4K, the mean fluorescence intensity of microglia was significantly higher one or three days after stroke ($p < 0.01$). QHRD106 treatment obviously reduced the fluorescence intensity one ($p < 0.01$) or three ($p < 0.05$) days after stroke. Compared with QHRD106 alone, HOE-140 nonsignificantly increased microglial fluorescence intensity. Taken together, these results indicated that QHRD106 could attenuate the activation of microglia after ischemic stroke.

QHRD106 decreased neuronal and microglial HMGB1 translocation and secretion *in vitro*

According to the *in vivo* results, we wondered whether QHRD106 could decrease the translocation and secretion of HMGB1 after stimulation in primary cortical neurons and primary microglial cells *in vitro*. As HMGB1 can be passively released by necrotic neurons, we first used a cell counting kit-8 (CCK-8) assay and calcein-AM/PI labeling to investigate the neuroprotective effect of QHRD106 on primary neurons. As shown in Figures 5A and 5B, cell viability determined by the CCK-8 assay was dramatically decreased after OGD/R, while treatment with 1 mM and 2 mM QHRD106 significantly increased cell viability. The results also indicated that up to 2 mM QHRD106 showed no toxic effect on primary cortical neurons. The Calcein-AM/PI Double Stain Kit showed that 1 mM QHRD106 treatment increased the percentage of live cells (green) after OGD/R (Figures 5C and 5D). Thus, 1 mM QHRD106 was selected for subsequent experiments. The levels of medium HMGB1 were detected by western blotting, reflecting the secretion levels of HMGB1. The location of HMGB1 was revealed by double immunofluorescence staining (Figures 5E–5H).
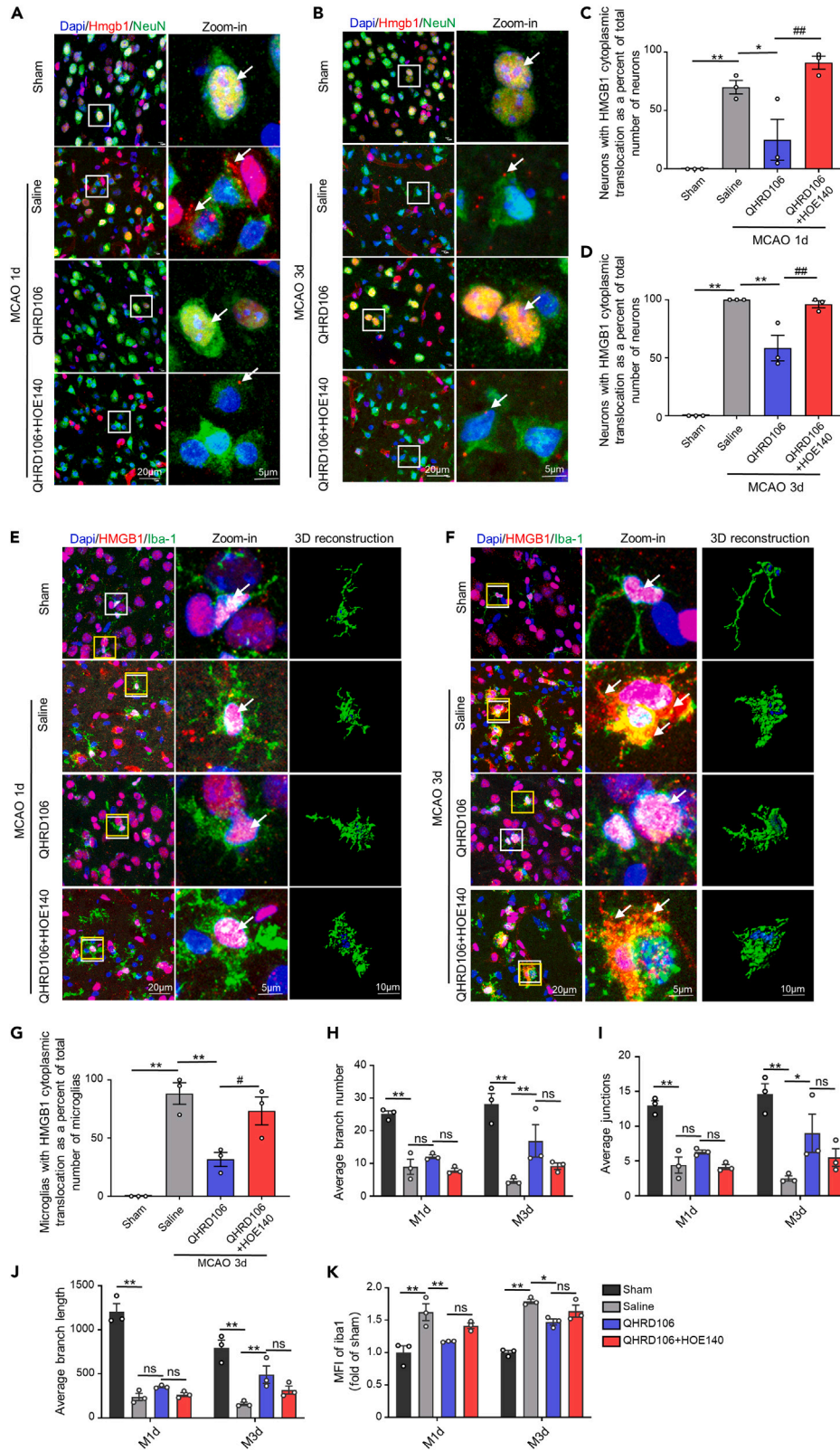
Figure 4. QHRD106 decreased neuronal and microglial HMGB1 translocation _in vivo_ via B2R

(A and B) Immunofluorescence of HMGB1 (red) in neuronal cells (NeuN$^+$; green) in the mouse ischemic penumbra 1 and 3 days after stroke. Arrows point to the location of HMGB1. The low-magnification illustration in the white box is displayed in the high-magnification view in the right column. DAPI staining is shown in blue.

(C and D) Quantification of the percentage of neurons with HMGB1 cytoplasmic translocation in total neurons of the ischemic penumbra 1 and 3 days after stroke.

(E and F) Immunofluorescence of HMGB1 (red) in microglial cells (Iba-1$^+$; green) in the mouse ischemic penumbra 1 and 3 days after stroke. The arrows point to the location of HMGB1. The low-magnification illustration in the white box is displayed in the high-magnification view in the right column. The microglia in the yellow box were selected for 3D reconstruction. DAPI staining is shown in blue.

(G) Quantification of the percentage of microglia with HMGB1 cytoplasmic translocation in total microglial cells of the ischemic penumbra 3 days after stroke.

(H–J) Confocal images were converted to binary images and then skeletonized. Microglial morphological analysis, including calculations of the average number of branches, average number of junctions, and average branch length, was performed with the Analyze Skeleton plugin of ImageJ.

(K) Quantification of the mean fluorescence intensity of Iba-1 1 and 3 days after stroke.

All data are presented as the mean $\pm$ SEM, n = 3/group. Statistical analyses were performed by one-way or two-way ANOVA with Tukey's post hoc test. *p < 0.05, **p < 0.01 vs. the saline group; #p < 0.05, ##p < 0.01 vs. the QHRD106 group, "ns" indicates no significance (p > 0.05).

Consistent with the _in vivo_ results, QHRD106 treatment significantly reduced the translocation and secretion of HMGB1 in primary neurons after OGD/R.

Considering the potential mechanism of the QHRD106-mediated anti-inflammatory response, the effect of QHRD106 treatment on primary microglia was investigated. LPS stimulation was used to mimic the inflammatory environment after ischemic stroke. Similar to the _in vivo_ results, the acetylation level of HMGB1 dramatically increased after 4 h of LPS stimulation, and QHRD106 significantly impeded the acetylation of HMGB1 (Figures S2C and S2D). In addition, HMGB1 levels in the microglial cytosol significantly increased after LPS stimulation, while QHRD106 treatment effectively decreased the translocation of HMGB1. There was no significant difference in nuclear HMGB1 expression among the three groups (Figures 5I–5K). Furthermore, QHRD106 treatment significantly reduced the secretion of HMGB1 after 24 h of LPS stimulation (Figures 5L and 5M). These results suggested that QHRD106 reduced both the passive release of HMGB1 by dying neurons and the active release of HMGB1 by LPS-stimulated microglia.

QHRD106 decreased microglial HMGB1 translocation and secretion by decreasing the binding between HMGB1 and HSP90AA1

To further elucidate the mechanisms of HMGB1 nucleocytoplasmic translocation, we examined the proteins interacting with HMGB1 in primary microglia using coimmunoprecipation (coIP), silver staining, and liquid chromatography-tandem mass spectrometry (LC-MS/MS) (Figure 6A). As shown in Figure 6B, HSP90AA1, a stress-inducible protein acting as a protein chaperone, was identified in LPS-stimulated primary microglia.[44,45] The protein-protein interaction (PPI) network among the HMGB1-binding proteins in the LPS group was predicted with STRING tools (Figure 6C). We hypothesized that QHRD106 might decrease microglial HMGB1 translocation and release after LPS stimulation by decreasing the binding between HMGB1 and HSP90AA1. First, we verified the binding relationship between HMGB1 and HSP90AA1 using a proximity ligation assay (PLA) and coIP (Figures 6D–6F). PLA showed that HMGB1 and HSP90AA1 interact in both the cytoplasm and nucleus of primary microglia. coIP showed that LPS stimulation significantly increased the binding between HMGB1 and HSP90AA1 and that QHRD106 decreased this binding relationship. We also verified through a PLA that QHRD106 decreased the interaction between HSP90AA1 and HMGB1 in the microglial cells of the mouse ischemic penumbra 3 days after stroke (Figures S3A and S3B).

Geldanamycin (GA), an HSP90AA1 inhibitor, was further used to inhibit the binding between HMGB1 and HSP90AA1. As shown in Figures 6G–6K, GA inhibited the translocation and secretion of HMGB1 after LPS stimulation in primary microglia, similar to those in the QHRD106 group. Therefore, we concluded that QHRD106 decreased the interaction between HSP90AA1 and HMGB1, thus decreasing the translocation and secretion of HMGB1 in microglial cells in an inflammatory environment.

DISCUSSION

The outcome of the ischemic penumbra is directly related to the prognosis of patients with ischemic stroke. Saving the ischemic penumbra is thus the key goal in the treatment of acute cerebral infarction. In the
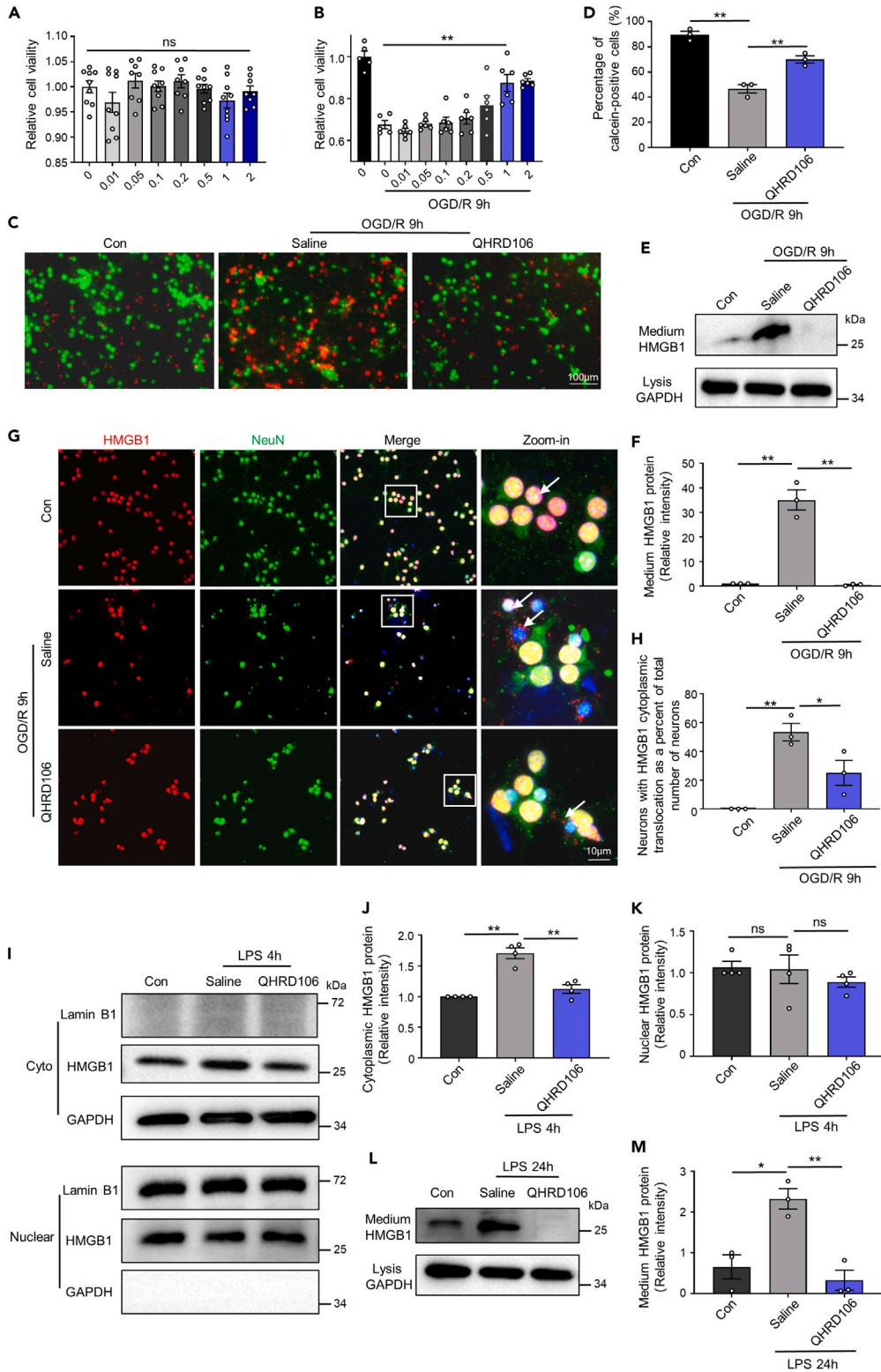
Figure 5. QHRD106 decreases neuronal and microglial HMGB1 secretion *in vitro*

(A and B) The CCK-8 method was used to determine the cell viability of *in vitro* primary neurons with the addition of 0–2 µM QHRD106. In addition, 1 µM QHRD106 was selected for *in vitro* experiments.

Figure 5. Continued

(C and D) The apoptosis of primary cortical neurons after OGD/R was evaluated by calcein-AM and PI dual labeling. Scale bar: 100 μm. Green fluorescent calcein-AM-positive cells indicated cell survival, and the percentage of these cells was calculated. n = 3/group. Statistical analyses were performed by one-way ANOVA with Tukey's post hoc test.

(E) Representative western blot images of medium HMGB1 and cell lysate GAPDH in primary cortical neurons 9 h after OGD/R.

(F) Quantification of medium HMGB1 expression.

(G and H) Immunofluorescence of HMGB1 (red) in neuronal cells (NeuN+; green) in primary cortical neurons 9 h after OGD/R. The arrows point to the location of HMGB1. The low-magnification illustration in the white box is displayed in the high-magnification view in the right column. DAPI staining is shown in blue, n = 3/group. Statistical analyses were performed by one-way ANOVA with Tukey's post hoc test.

(I–K) The nucleocytoplasmic translocation of HMGB1 in primary microglia 4 h after LPS (100 ng/mL) stimulation was evaluated by western blot analysis. GAPDH and Lamin B1 were used as cytoplasmic and nuclear loading controls, respectively.

(L) Representative western blot images of medium HMGB1 and cell lysis GAPDH in primary microglia 24 h after LPS stimulation.

(M) Quantification of medium HMGB1 expression.

All data are presented as the mean ± SEM. Statistical analyses were performed by one-way ANOVA followed by Tukey's post hoc test. *p < 0.05, **p < 0.01 vs. the saline group; "ns" indicates no significance (p > 0.05).

present study, we monitored the changes in neurological deficits and cerebral infarct volume in mice after MCAO, the most commonly used model to simulate human ischemic stroke, and the results showed that QHRD106, a long-acting TK, effectively attenuated the brain infarct size and improved cerebral damage through B2R instead of B1R. We found that QHRD106 reduced apoptosis and neuroinflammation. The proteomics experiment results showed that the underlying mechanism involved abnormal distribution and expression of HMGB1. These findings were verified in primary cortical neurons and microglial cells and *in vivo*. QHRD106 reduced either the passive release of HMGB1 by reducing neuronal death or the active release of HMGB1 by reducing microglial activation. Further studies showed that QHRD106 decreased HMGB1 translocation and secretion by inhibiting the level of acetylated HMGB1 and decreasing the binding between HSP90AA1 and HMGB1. A mechanistic model of the protective effects of QHRD106 is illustrated in the graphical abstract.

Human urinary kallidinogenase (HUK), a TK derived from human urine that regulates KKS, has been listed as a national category I new drug approved by China's State Food and Drug Administration, and it is widely used for the treatment of stroke patients in China. Our previous clinical and animal studies have shown that treatment with HUK improves stroke outcomes in patients,[46] promotes postischemic angiogenesis, and suppresses inflammatory responses and brain edema in mice via activation of BK receptors and inhibition of the NF-κB signaling pathways.[47,48] Although both QHRD106 and HUK are TKs, QHRD106 has several advantages over HUK, mainly due to the short half-life of HUK, which necessitates daily intravenous infusion during clinical treatment and animal models and thus increases the pain caused to subjects.[48,49] PEG modification prolongs the half-life of QHRD106, and QHRD106 is administered by intramuscular injection, reducing the number of administrations and further improving the convenience of clinical use and animal testing. In addition, QHRD106 is a TK extracted from the pig pancreas by purification. Therefore, the supply of raw material for QHRD106 production is plentiful, suggesting that this drug may be a promising candidate to treat ischemic stroke.

The effects of TK are mediated by the BK receptors B1R and B2R. B1R is usually absent from healthy tissue, but B2R is widely expressed throughout the body.[50] Both receptors are upregulated after cerebral ischemia-reperfusion, but the role of B1R and B2R in ischemic stroke is controversial.[32,51,52] In the current experiments, the ischemic brain protection induced by QHRD106 injection was blocked by combination treatment with the B2R antagonist HOE-140 but not by combination treatment with the B1R antagonist R-715. This phenomenon suggests that B1R and B2R may play different roles after ischemic brain injury, which is consistent with a report demonstrating that B1R inhibition reduces infarct volume, while B2R antagonism exacerbates blood brain barrier (BBB) damage and neuroinflammation in diabetic cerebral ischemia.[51] Another study found that simultaneous inhibition of B1R and B2R or inhibition of B2R alone reverses the neuroprotective effect of HUK, suggesting that the BK-induced protective effect is mainly mediated by B2R.[34] Furthermore, structural studies have revealed that the binding of BK to B2R is over 10,000-fold that of B1R,[53,54] so we believe that QHRD106 protects against ischemic brain injury mainly through activation of B2R.

A

B

Band number	Protein HSP90AA1	Accession number	Molecular weight
1	Not detected		
2	Detected	P07901	84.7

C

D

E

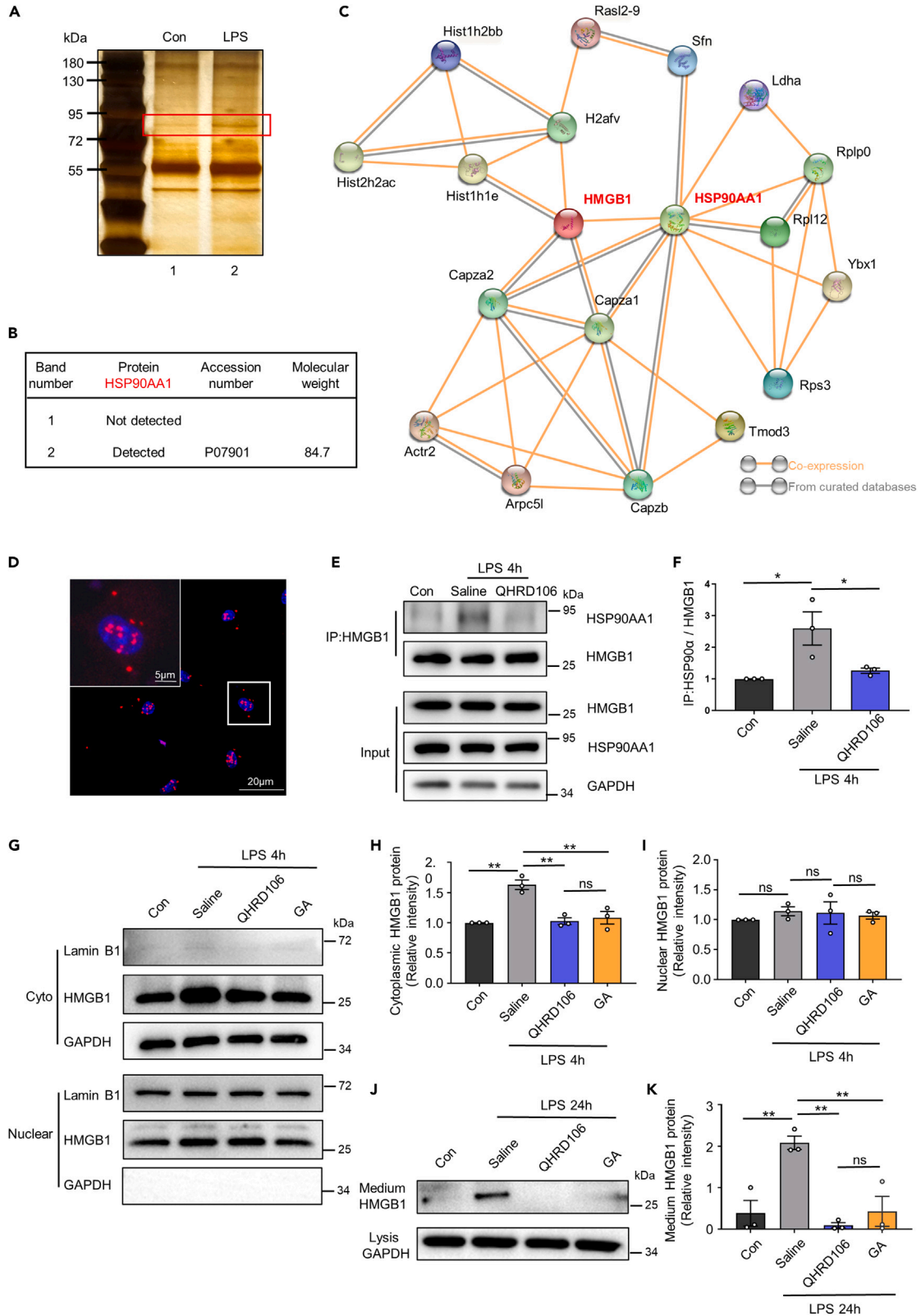

F

G

H

I

J

K

Figure 6. QHRD106 decreased microglial HMGB1 translocation and secretion by decreasing the binding between HMGB1 and HSP90AA1

(A–C) Primary microglial cells were treated with LPS for 4 h, the whole lysates were mixed with anti-HMGB1-coated Protein A/G PLUS-agarose beads, and the HMGB1-binding protein was subjected to SDS/PAGE. (A) The gel of the complex was stained by silver staining and analyzed by LC-MS/MS. (B) HSP90AA1 was identified in LPS-stimulated primary microglia. (C) The PPI network among the HMGB1-binding proteins in the LPS group was predicted with STRING tools.

(D) Primary microglial cells were treated with LPS for 4 h, and the interaction between HMGB1 and HSP90AA1 was observed using PLA.

(E and F) To observe the interaction between HMGB1 and HSP90AA1, whole-cell lysates in the control, saline, and QHRD106 groups were immunoprecipitated and immunoblotted.

(G–K) QHRD106 at 1 μM or GA at 0.2 μM was added.(G–I) The nucleocytoplasmic translocation of HMGB1 in primary microglia 4 h after LPS stimulation was evaluated by western blot analysis. GAPDH and Lamin B1 were used as cytoplasmic and nuclear loading controls, respectively. (J) Representative western blot images of medium HMGB1 and cell lysis GAPDH in primary microglia 24 h after LPS stimulation. (K) Quantification of medium HMGB1 expression. All data are presented as the mean ± SEM. Statistical analyses were performed by one-way ANOVA followed by Tukey's post hoc test. *p < 0.05, **p < 0.01 vs. the saline group; "ns" indicates no significance (p > 0.05).

HMGB1, acting as a key inflammatory mediator, has been proven to mediate a range of diseases, such as ischemic stroke, Alzheimer's disease (AD), Parkinson's disease (PD), and multiple sclerosis (MS).[55–57] It has been suggested that released HMGB1 further exacerbates inflammation and apoptosis after ischemic stroke.[16–19] In addition, various studies have demonstrated that extracellular HMGB1 plays an important role in neutrophil extracellular trap formation, platelet activation, and subsequent thrombosis,[58] which is corroborated by the KEGG and GO analyses in our proteomics experiments. Therefore, we believe that a decrease in HMGB1 may be a key factor in the protective effect of QHRD106 after ischemic stroke.

Research has demonstrated that microglia and neurons are the main cell sources of HMGB1 in animal depressive models and ischemic stroke, and HMGB1 can be secreted into the extracellular environment by activated microglia and dying neurons.[22,59] Elevated serum or extracellular HMGB1 has also been observed in clinical studies and animal models of ischemic stroke.[24,25] Although clinical studies on HMGB1 interventions are lacking, inhibition of HMGB1 has shown beneficial effects in animal models of ischemic stroke.[27,29,60] Our results showed that QHRD106 decreased the translocation of nuclear HMGB1 in the penumbral tissue after stroke. The results of double immunofluorescence staining demonstrated that both neurons and microglia are able to secrete HMGB1 after stroke and that QHRD106 can reduce both passive release of HMGB1 by necrotic neurons and active release of HMGB1 by microglia *in vivo* and *in vitro*.

The mechanism of HMGB1 translocation is very complicated. Many studies have indicated that hyperacetylation of HMGB1 affects its DNA binding activity and induces its translocation and secretion.[16,30,31] The results presented here show that QHRD106 significantly reduces the levels of HMGB1 acetylation in infarcted brain penumbral tissue after MCAO and in LPS-stimulated microglial cells. Chen et al. found that luteolin, an inhibitor of HSP90, destabilized the Hsp90 client proteins c-Jun and Akt and subsequently reduced HMGB1 release in a sepsis model.[61] In addition, a recently published study showed that HSP90AA1 regulated the translocation and secretion of HMGB1 in HEK293T cells through direct interaction, suggesting that HSP90AA1 may act as an upstream regulator of HMGB1.[62] Consistent with these findings, the results of coIP followed by LC-MS/MS found that the binding of HSP90AA1 and HMGB1 increased in activated microglia, while QHRD106 weakened their binding. HMGB1 translocation and secretion were both decreased by QHRD106 or an inhibitor of HSP90AA1 in activated microglia. Our study is the first to confirm that HSP90AA1 may be another important mechanism of HMGB1 translocation in addition to acetylation after ischemic stroke.

Limitations of the study

One limitation of our study is that the current experiment focused only on the acute phase of ischemic stroke (1–7 days). Whether QHRD106 exerts neuroprotective effects for an extended period after ischemic brain injury, such as up to 30 days, remains to be investigated. Another possible limitation is that although QHRD106 inhibited neuronal death after ischemia, which is consistent with numerous studies showing that TK can promote neuronal survival,[33,34,37] the underlying mechanism remains to be identified.

STAR★METHODS

Detailed methods are provided in the online version of this paper and include the following:

- KEY RESOURCES TABLE

SUPPLEMENTAL INFORMATION

Supplemental information can be found online at https://doi.org/10.1016/j.isci.2023.107268.

AUTHOR CONTRIBUTIONS

Y.X. and X.C. designed the project. S-y.X., J.J., M.S., X.B., and S-n.X. performed the experiments and analyzed the data. Y.X. and X.C. contributed reagents and materials. S-y.X., J.J., and X.C. wrote the manuscript. S.S., S.J., P.L., and L.Y. revised the manuscript. All the authors read and approved the final version of the manuscript.

DECLARATION OF INTERESTS

The authors declare no competing interests.

REFERENCES

1. Ajoolabady, A., Wang, S., Kroemer, G., Penninger, J.M., Uversky, V.N., Pratico, D., Henninger, N., Reiter, R.J., Bruno, A., Joshipura, K., et al. (2021). Targeting autophagy in ischemic stroke: from molecular mechanisms to clinical therapeutics. Pharmacol. Ther. *225*, 107848. https://doi.org/10.1016/j.pharmthera.2021.107848.

2. Nimjee, S.M., Akhter, A.S., Zakeri, A., and Herson, P.S. (2022). Sex differences in thrombosis as it affects acute ischemic stroke. Neurobiol. Dis. *165*, 105647. https://doi.org/10.1016/j.nbd.2022.105647.

3. Campbell, B.C.V., De Silva, D.A., Macleod, M.R., Coutts, S.B., Schwamm, L.H., Davis, S.M., and Donnan, G.A. (2019). Ischaemic

stroke. Nat. Rev. Dis. Prim. *5*, 70. https://doi.org/10.1038/s41572-019-0118-8.

4. Huang, S.S., Su, H.H., Chien, S.Y., Chung, H.Y., Luo, S.T., Chu, Y.T., Wang, Y.H., MacDonald, I.J., Lee, H.H., and Chen, Y.H. (2022). Activation of peripheral TRPM8 mitigates ischemic stroke by topically applied menthol. J. Neuroinflammation *19*, 192. https://doi.org/10.1186/s12974-022-02553-4.

5. Luo, L., Liu, M., Fan, Y., Zhang, J., Liu, L., Li, Y., Zhang, Q., Xie, H., Jiang, C., Wu, J., et al. (2022). Intermittent theta-burst stimulation improves motor function by inhibiting neuronal pyroptosis and regulating microglial polarization via TLR4/NFκB/NLRP3 signaling pathway in cerebral ischemic mice. J. Neuroinflammation *19*, 141. https://doi.org/10.1186/s12974-022-02501-2.

6. Lambertsen, K.L., Finsen, B., and Clausen, B.H. (2019). Post-stroke inflammation-target or tool for therapy? Acta Neuropathol. *137*, 693–714. https://doi.org/10.1007/s00401-018-1930-z.

7. Albers, G.W., Marks, M.P., and Lansberg, M.G. (2018). Thrombectomy for Stroke with selection by perfusion imaging. N. Engl. J. Med. *378*, 1849–1850. https://doi.org/10.1056/NEJMc1803856.

8. Nogueira, R.G., Jadhav, A.P., Haussen, D.C., Bonafe, A., Budzik, R.F., Bhuva, P., Yavagal, D.R., Ribo, M., Cognard, C., Hanel, R.A., et al. (2018). Thrombectomy 6 to 24 hours after stroke with a mismatch between deficit and infarct. N. Engl. J. Med. *378*, 11–21. https://doi.org/10.1056/NEJMoa1706442.

9. Ma, Y., Wang, J., Wang, Y., and Yang, G.Y. (2017). The biphasic function of microglia in ischemic stroke. Prog. Neurobiol. *157*, 247–272. https://doi.org/10.1016/j.pneurobio.2016.01.005.

10. Cai, G., Cai, G., Zhou, H., Zhuang, Z., Liu, K., Pei, S., Wang, Y., Wang, H., Wang, X., Xu, S., et al. (2021). Mesenchymal stem cell-derived exosome miR-542-3p suppresses inflammation and prevents cerebral infarction. Stem Cell Res. Ther. *12*, 2. https://doi.org/10.1186/s13287-020-02030-w.

11. Tian, X., Liu, C., Shu, Z., and Chen, G. (2017). Review: therapeutic targeting of HMGB1 in stroke. Curr. Drug Deliv. *14*, 785–790. https://doi.org/10.2174/1567201813666160808111933.

12. Eide, S., and Feng, Z.-P. (2022). Implications of age-related changes in the blood-brain barrier for ischemic stroke and new treatment strategies. Adv. Neuro. *1*, 1. https://doi.org/10.36922/an.v1i2.1.

13. Zhang, B., Zhang, H.X., Shi, S.T., Bai, Y.L., Zhe, X., Zhang, S.J., and Li, Y.J. (2019). Interleukin-11 treatment protected against cerebral ischemia/reperfusion injury. Biomed. Pharmacother. *115*, 108816. https://doi.org/10.1016/j.biopha.2019.108816.

14. Yuan, J., Li, L., Yang, Q., Ran, H., Wang, J., Hu, K., Pu, W., Huang, J., Wen, L., Zhou, L., et al. (2021). Targeted treatment of ischemic stroke by bioactive nanoparticle-derived reactive oxygen species responsive and inflammation-resolving nanotherapies. ACS Nano *15*, 16076–16094. https://doi.org/10.1021/acsnano.1c04753.

15. Xue, J., Suarez, J.S., Minaai, M., Li, S., Gaudino, G., Pass, H.I., Carbone, M., and Yang, H. (2021). HMGB1 as a therapeutic target in disease. J. Cell. Physiol. *236*, 3406–3419. https://doi.org/10.1002/jcp.30125.

16. Chen, R., Kang, R., and Tang, D. (2022). The mechanism of HMGB1 secretion and release. Exp. Mol. Med. *54*, 91–102. https://doi.org/10.1038/s12276-022-00736-w.

17. Kim, S.W., Lim, C.M., Kim, J.B., Shin, J.H., Lee, S., Lee, M., and Lee, J.K. (2011). Extracellular HMGB1 released by NMDA treatment confers neuronal apoptosis via RAGE-p38 MAPK/ERK signaling pathway. Neurotox. Res. *20*, 159–169. https://doi.org/10.1007/s12640-010-9231-x.

18. Mi, L., Zhang, Y., Xu, Y., Zheng, X., Zhang, X., Wang, Z., Xue, M., and Jin, X. (2019). HMGB1/RAGE pro-inflammatory axis promotes vascular endothelial cell apoptosis in limb ischemia/reperfusion injury. Biomed. Pharmacother. *116*, 109005. https://doi.org/10.1016/j.biopha.2019.109005.

19. Liu, B., Gan, X., Zhao, Y., Gao, J., and Yu, H. (2021). Inhibition of HMGB1 reduced high glucose-induced BMSCs apoptosis via activation of AMPK and regulation of mitochondrial functions. J. Physiol. Biochem. *77*, 227–235. https://doi.org/10.1007/s13105-021-00784-2.

20. Kim, J.B., Lim, C.M., Yu, Y.M., and Lee, J.K. (2008). Induction and subcellular localization of high-mobility group box-1 (HMGB1) in the postischemic rat brain. J. Neurosci. Res. *86*, 1125–1131. https://doi.org/10.1002/jnr.21555.

21. Xiong, X.X., Gu, L.J., Shen, J., Kang, X.H., Zheng, Y.Y., Yue, S.B., and Zhu, S.M. (2014). Probenecid protects against transient focal cerebral ischemic injury by inhibiting HMGB1 release and attenuating AQP4 expression in mice. Neurochem. Res. *39*, 216–224. https://doi.org/10.1007/s11064-013-1212-z.

22. Qiu, J., Nishimura, M., Wang, Y., Sims, J.R., Qiu, S., Savitz, S.I., Salomone, S., and Moskowitz, M.A. (2008). Early release of HMGB-1 from neurons after the onset of brain ischemia. J. Cerebr. Blood Flow Metabol. *28*, 927–938. https://doi.org/10.1038/sj.jcbfm.9600582.

23. Ye, Y., Zeng, Z., Jin, T., Zhang, H., Xiong, X., and Gu, L. (2019). The role of high mobility group box 1 in ischemic stroke. Front. Cell. Neurosci. *13*, 127. https://doi.org/10.3389/fncel.2019.00127.

24. Schulze, J., Zierath, D., Tanzi, P., Cain, K., Shibata, D., Dressel, A., and Becker, K. (2013). Severe stroke induces long-lasting alterations of high-mobility group box 1. Stroke *44*, 246–248. https://doi.org/10.1161/strokeaha.112.676072.

25. Kim, J.B., Sig Choi, J., Yu, Y.M., Nam, K., Piao, C.S., Kim, S.W., Lee, M.H., Han, P.L., Park, J.S., and Lee, J.K. (2006). HMGB1, a novel cytokine-like mediator linking acute neuronal death and delayed neuroinflammation in the postischemic brain. J. Neurosci. *26*, 6413–6421. https://doi.org/10.1523/jneurosci.3815-05.2006.

26. Xie, W., Zhu, T., Dong, X., Nan, F., Meng, X., Zhou, P., Sun, G., and Sun, X. (2019). HMGB1-triggered inflammation inhibition of notoginseng leaf triterpenes against cerebral ischemia and reperfusion injury via MAPK and NF-κB signaling pathways. Biomolecules *9*, 512. https://doi.org/10.3390/biom9100512.

27. Chen, H., Guan, B., Wang, B., Pu, H., Bai, X., Chen, X., Liu, J., Li, C., Qiu, J., Yang, D., et al. (2020). Glycyrrhizin prevents hemorrhagic transformation and improves neurological outcome in ischemic stroke with delayed thrombolysis through targeting peroxynitrite-mediated HMGB1 signaling. Transl. Stroke Res. *11*, 967–982. https://doi.org/10.1007/s12975-019-00772-1.

28. Gong, G., Xiang, L., Yuan, L., Hu, L., Wu, W., Cai, L., Yin, L., and Dong, H. (2014). Protective effect of glycyrrhizin, a direct HMGB1 inhibitor, on focal cerebral ischemia/reperfusion-induced inflammation, oxidative stress, and apoptosis in rats. PLoS One *9*, e89450. https://doi.org/10.1371/journal.pone.0089450.

29. Tao, X., Sun, X., Yin, L., Han, X., Xu, L., Qi, Y., Xu, Y., Li, H., Lin, Y., Liu, K., and Peng, J. (2015). Dioscin ameliorates cerebral ischemia/reperfusion injury through the downregulation of TLR4 signaling via HMGB-1 inhibition. Free Radic. Biol. Med. *84*, 103–115. https://doi.org/10.1016/j.freeradbiomed.2015.03.003.

30. Scaffidi, P., Misteli, T., and Bianchi, M.E. (2002). Release of chromatin protein HMGB1 by necrotic cells triggers inflammation. Nature *418*, 191–195. https://doi.org/10.1038/nature00858.

31. Chen, X., Chen, C., Fan, S., Wu, S., Yang, F., Fang, Z., Fu, H., and Li, Y. (2018). Omega-3 polyunsaturated fatty acid attenuates the inflammatory response by modulating microglia polarization through SIRT1-mediated deacetylation of the HMGB1/NF-κB pathway following experimental traumatic brain injury. J. Neuroinflammation *15*, 116. https://doi.org/10.1186/s12974-018-1151-3.

32. Nokkari, A., Abou-El-Hassan, H., Mechref, Y., Mondello, S., Kindy, M.S., Jaffa, A.A., and Kobeissy, F. (2018). Implication of the Kallikrein-Kinin system in neurological disorders: quest for potential biomarkers and mechanisms. Prog. Neurobiol. *165–167*, 26–50. https://doi.org/10.1016/j.pneurobio.2018.01.003.

33. Su, J., Tang, Y., Zhou, H., Liu, L., and Dong, Q. (2012). Tissue kallikrein protects neurons from hypoxia/reoxygenation-induced cell injury through Homer1b/c. Cell. Signal. *24*, 2205–2215. https://doi.org/10.1016/j.cellsig.2012.04.021.

34. Shi, R., Yuan, K., Hu, B., Sang, H., Zhou, L., Xie, Y., Xu, L., Cao, Q., Chen, X., Zhao, L., et al. (2016). Tissue Kallikrein alleviates cerebral ischemia-reperfusion injury by activating the B2R-ERK1/2-CREB-Bcl-2 signaling pathway in diabetic rats. Oxid. Med. Cell. Longev. *2016*,

1843201. https://doi.org/10.1155/2016/1843201.

35. Alexander-Curtis, M., Pauls, R., Chao, J., Volpi, J.J., Bath, P.M., and Verdoorn, T.A. (2019). Human tissue kallikrein in the treatment of acute ischemic stroke. Ther. Adv. Neurol. Disord. 12, 1756286418821918. https://doi.org/10.1177/1756286418821918.

36. Zhao, Z., Xu, Z., Liu, T., Huang, S., Huang, H., and Huang, X. (2019). Human urinary kallidinogenase reduces lipopolysaccharide-induced neuroinflammation and oxidative stress in BV-2 cells. Pain Res. Manag. 2019, 6393150. https://doi.org/10.1155/2019/6393150.

37. Liu, Y., Lu, Z., Cui, M., Yang, Q., Tang, Y., and Dong, Q. (2016). Tissue kallikrein protects SH-SY5Y neuronal cells against oxygen and glucose deprivation-induced injury through bradykinin B2 receptor-dependent regulation of autophagy induction. J. Neurochem. 139, 208–220. https://doi.org/10.1111/jnc.13690.

38. Ren, W., and Yang, X. (2018). Pathophysiology of long non-coding RNAs in ischemic stroke. Front. Mol. Neurosci. 11, 96. https://doi.org/10.3389/fnmol.2018.00096.

39. Kim, S.W., Lee, H., Lee, H.K., Kim, I.D., and Lee, J.K. (2019). Neutrophil extracellular trap induced by HMGB1 exacerbates damages in the ischemic brain. Acta Neuropathol. Commun. 7, 94. https://doi.org/10.1186/s40478-019-0747-x.

40. Tsukagawa, T., Katsumata, R., Fujita, M., Yasui, K., Akhoon, C., Ono, K., Dohi, K., and Aruga, T. (2017). Elevated serum high-mobility group box-1 protein level is associated with poor functional outcome in ischemic stroke. J. Stroke Cerebrovasc. Dis. 26, 2404–2411. https://doi.org/10.1016/j.jstrokecerebrovasdis.2017.05.033.

41. Mota, M., Porrini, V., Parrella, E., Benarese, M., Bellucci, A., Rhein, S., Schwaninger, M., and Pizzi, M. (2020). Neuroprotective epi-drugs quench the inflammatory response and microglial/macrophage activation in a mouse model of permanent brain ischemia. J. Neuroinflammation 17, 361. https://doi.org/10.1186/s12974-020-02028-4.

42. Morrison, H.W., and Filosa, J.A. (2013). A quantitative spatiotemporal analysis of microglia morphology during ischemic stroke and reperfusion. J. Neuroinflammation 10, 4. https://doi.org/10.1186/1742-2094-10-4.

43. Bonsack, F., 4th, Alleyne, C.H., Jr., and Sukumari-Ramesh, S. (2016). Augmented expression of TSPO after intracerebral hemorrhage: a role in inflammation? J. Neuroinflammation 13, 151. https://doi.org/10.1186/s12974-016-0619-2.

44. Schopf, F.H., Biebl, M.M., and Buchner, J. (2017). The HSP90 chaperone machinery. Nat. Rev. Mol. Cell Biol. 18, 345–360. https://doi.org/10.1038/nrm.2017.20.

45. Pearl, L.H., and Prodromou, C. (2006). Structure and mechanism of the Hsp90 molecular chaperone machinery. Annu. Rev. Biochem. 75, 271–294. https://doi.org/10.1146/annurev.biochem.75.103004.142738.

46. Li, J., Chen, Y., Zhang, X., Zhang, B., Zhang, M., and Xu, Y. (2015). Human urinary kallidinogenase improves outcome of stroke patients by shortening mean transit time of perfusion magnetic resonance imaging. J. Stroke Cerebrovasc. Dis. 24, 1730–1737. https://doi.org/10.1016/j.jstrokecerebrovasdis.2015.03.032.

47. Han, L., Li, J., Chen, Y., Zhang, M., Qian, L., Chen, Y., Wu, Z., Xu, Y., and Li, J. (2015). Human urinary kallidinogenase promotes angiogenesis and cerebral perfusion in experimental stroke. PLoS One 10, e0134543. https://doi.org/10.1371/journal.pone.0134543.

48. Chen, Z.B., Huang, D.Q., Niu, F.N., Zhang, X., Li, E.G., and Xu, Y. (2010). Human urinary kallidinogenase suppresses cerebral inflammation in experimental stroke and downregulates nuclear factor-kappaB. J. Cerebr. Blood Flow Metabol. 30, 1356–1365. https://doi.org/10.1038/jcbfm.2010.19.

49. Han, D., Chen, X., Li, D., Liu, S., Lyu, Y., and Feng, J. (2018). Human urinary Kallidinogenase decreases recurrence risk and promotes good recovery. Brain Behav. 8, e01033. https://doi.org/10.1002/brb3.1033.

50. Lau, J., Rousseau, J., Kwon, D., Bénard, F., and Lin, K.S. (2020). A systematic review of molecular imaging agents targeting bradykinin B1 and B2 receptors. Pharmaceuticals 13, 199. https://doi.org/10.3390/ph13080199.

51. Sang, H., Liu, L., Wang, L., Qiu, Z., Li, M., Yu, L., Zhang, H., Shi, R., Yu, S., Guo, R., et al. (2016). Opposite roles of bradykinin B1 and B2 receptors during cerebral ischaemia-reperfusion injury in experimental diabetic rats. Eur. J. Neurosci. 43, 53–65. https://doi.org/10.1111/ejn.13133.

52. Desposito, D., Zadigue, G., Taveau, C., Adam, C., Alhenc-Gelas, F., Bouby, N., and Roussel, R. (2017). Neuroprotective effect of kinin B1 receptor activation in acute cerebral ischemia in diabetic mice. Sci. Rep. 7, 9410. https://doi.org/10.1038/s41598-017-09721-0.

53. Yin, Y.L., Ye, C., Zhou, F., Wang, J., Yang, D., Yin, W., Wang, M.W., Xu, H.E., and Jiang, Y. (2021). Molecular basis for kinin selectivity and activation of the human bradykinin receptors. Nat. Struct. Mol. Biol. 28, 755–761. https://doi.org/10.1038/s41594-021-00645-y.

54. Leeb-Lundberg, L.M.F., Marceau, F., Müller-Esterl, W., Pettibone, D.J., and Zuraw, B.L. (2005). International union of pharmacology. XLV. Classification of the kinin receptor family: from molecular mechanisms to pathophysiological consequences. Pharmacol. Rev. 57, 27–77. https://doi.org/10.1124/pr.57.1.2.

55. Paudel, Y.N., Angelopoulou, E., Piperi, C., Othman, I., Aamir, K., and Shaikh, M.F. (2020). Impact of HMGB1, RAGE, and TLR4 in Alzheimer's Disease (AD): from risk factors to therapeutic targeting. Cells 9, 383. https://doi.org/10.3390/cells9020383.

56. Tian, Y., Chen, R., and Su, Z. (2023). HMGB1 is a potential and challenging therapeutic target for Parkinson's Disease. Cell. Mol. Neurobiol. 43, 47–58. https://doi.org/10.1007/s10571-021-01170-8.

57. Paudel, Y.N., Angelopoulou, E., C, B.K., Piperi, C., and Othman, I. (2019). High mobility group box 1 (HMGB1) protein in Multiple Sclerosis (MS): mechanisms and therapeutic potential. Life Sci. 238, 116924. https://doi.org/10.1016/j.lfs.2019.116924.

58. Kim, S.W., and Lee, J.K. (2020). Role of HMGB1 in the interplay between NETosis and thrombosis in ischemic stroke: a review. Cells 9, 1794. https://doi.org/10.3390/cells9081794.

59. Wang, B., Huang, X., Pan, X., Zhang, T., Hou, C., Su, W.J., Liu, L.L., Li, J.M., and Wang, Y.X. (2020). Minocycline prevents the depressive-like behavior through inhibiting the release of HMGB1 from microglia and neurons. Brain Behav. Immun. 88, 132–143. https://doi.org/10.1016/j.bbi.2020.06.019.

60. Zhang, J., Takahashi, H.K., Liu, K., Wake, H., Liu, R., Maruo, T., Date, I., Yoshino, T., Ohtsuka, A., Mori, S., and Nishibori, M. (2011). Anti-high mobility group box-1 monoclonal antibody protects the blood-brain barrier from ischemia-induced disruption in rats. Stroke 42, 1420–1428. https://doi.org/10.1161/strokeaha.110.598334.

61. Chen, D., Bi, A., Dong, X., Jiang, Y., Rui, B., Liu, J., Yin, Z., and Luo, L. (2014). Luteolin exhibits anti-inflammatory effects by blocking the activity of heat shock protein 90 in macrophages. Biochem. Biophys. Res. Commun. 443, 326–332. https://doi.org/10.1016/j.bbrc.2013.11.122.

62. Kim, Y.H., Kwak, M.S., Lee, B., Shin, J.M., Aum, S., Park, I.H., Lee, M.G., and Shin, J.S. (2021). Secretory autophagy machinery and vesicular trafficking are involved in HMGB1 secretion. Autophagy 17, 2345–2362. https://doi.org/10.1080/15548627.2020.1826690.

63. Meng, H., Zhao, H., Cao, X., Hao, J., Zhang, H., Liu, Y., Zhu, M.S., Fan, L., Weng, L., Qian, L., et al. (2019). Double-negative T cells remarkably promote neuroinflammation after ischemic stroke. Proc. Natl. Acad. Sci. USA 116, 5558–5563. https://doi.org/10.1073/pnas.1814394116.

64. Young, K., and Morrison, H. (2018). Quantifying microglia morphology from photomicrographs of immunohistochemistry prepared tissue using ImageJ. J. Vis. Exp. 57648. https://doi.org/10.3791/57648.

STAR★METHODS

KEY RESOURCES TABLE

REAGENT or RESOURCE	SOURCE	IDENTIFIER
Antibodies		
Rabbit anti-Bax	Bioworld	Cat#BS2538; RRID:AB_1663713
Rabbit anti-Bcl-2	Bioworld	Cat#BS1511; RRID:AB_1663933
Mouse anti-iNOS	BD Biosciences	Cat#610328; RRID:AB_397718
Mouse anti-MCP-1	Proteintech	Cat#66272-1-Ig; RRID:AB_2861337
Rabbit anti-TNF-α	Proteintech	Cat#17590-1-AP; RRID:AB_2271853
Rabbit anti-β-actin	Bioworld	Cat#AP0060; RRID:AB_2797445
Rabbit anti-Lamin B1	Bioworld	Cat#AP6001; RRID:AB_2797499
Rabbit anti-HMGB1	Abcam	Cat#ab18256; RRID:AB_444360
Rabbit anti-GAPDH	Bioworld	Cat#AP0063; RRID:AB_2651132
Rabbit anti-Acetyllysine	PTM-BioLab	Cat#PTM-105; RRID:AB_2877698
Rabbit anti-HSP90AA1	Invitrogen	Cat#PA3-013; RRID:AB_2120934
Mouse anti-HSP90AA1	Proteintech	Cat#60318-1-Ig
Mouse anti-NeuN	Abcam	Cat#ab104224; RRID:AB_10711040
Goat anti-Iba-1	Abcam	Cat#ab5076; RRID:AB_2224402
Goat anti-rabbit IgG (H + L) secondary antibody, HRP	Bioworld	Cat#BS13278; RRID:AB_2773728
Goat anti-mouse IgG (H + L) secondary antibody, HRP	Bioworld	Cat#BS12478; RRID:AB_2773727
Donkey anti-goat, Alexa Fluor 488	Invitrogen	Cat#A11055; RRID:AB_2534102
Donkey anti-mouse, Alexa Fluor 488	Invitrogen	Cat#A21202; RRID:AB_141607
Donkey anti-rabbit, Alexa Fluor 594	Invitrogen	Cat#A21207; RRID:AB_141637
Donkey anti-mouse, Alexa Fluor 594	Invitrogen	Cat#A21203; RRID:AB_141633
Chemicals, peptides, and recombinant proteins		
HOE-140	MedChemExpress	Cat#HY-17446
Geldanamycin	MedChemExpress	Cat#HY-15230
R-715	Tocris Bioscience	Cat#3407
LPS	Sigma-Aldrich	L6529
Deposited data		
Proteomics analysis	N/A	Accession number: PXD042777
Interactome analysis	N/A	Accession number: PXD042778
Experimental models: Organisms/strains		
Mouse: C57/BL6J	the Model Animal Research Center of Nanjing University	N/A
Oligonucleotides		
Nos2	TsingkeBiotechnologyCo.,Ltd.	F:CAGCTGGGCTGTACAAACCTT R: CATTGGAAGTGAAGCGTTTCG
Il6	TsingkeBiotechnologyCo.,Ltd.	F:GCTGGTGACAACCACGGCCT R: AGCCTCCGACTTGTGAAGTGGT
Tnfa	TsingkeBiotechnologyCo.,Ltd.	F:CAAGGGACAAGGCTGCCCCG R:GCAGGGGGCTCTTGACGGCAG

Continued

REAGENT or RESOURCE	SOURCE	IDENTIFIER
Ccl2	TsingkeBiotechnologyCo.,Ltd.	F: TTGAGGTGGTTGTGGAAAAGG R:GTGCTGACCCCAAGAAGGAAT
Il1b	TsingkeBiotechnologyCo.,Ltd.	F:AAGCCTCGTGCTGTCGGACC R:TGAGGCCCAAGGCCACAGG
Il10	TsingkeBiotechnologyCo.,Ltd.	F:GGTTGCCAAGCCTTATCGGA R:ACCTGCTCCACTGCCTTGCT
Gapdh	TsingkeBiotechnologyCo.,Ltd.	F:GCCAAGGCTGTGGGCAAGGT R:TCTCCAGGCGGCACGTCAGA
Software and algorithms		
ImageJ	NIH	N/A
Prism	GraphPad	N/A
Adobe Illustrator CS6	Adobe Systems	N/A

RESOURCE AVAILABILITY

Lead contact

Further information and requests for resources and reagents should be directed to and will be fulfilled by the lead contact, Yun Xu (xuyun20042001@aliyun.com).

Materials availability

This study did not generate new unique reagents.

Data and code availability

- Data reported in this paper will be shared by the lead contact upon request.

- The mass spectrometry proteomics data have been deposited to the ProteomeXchange Consortium (http://proteomecentral.proteomexchange.org) via the iProX partner repository with the dataset identifier PXD042777 and PXD042778 and are publicly available as of the date of publication. Accession numbers are listed in the key resources table.

- This paper does not report original code.

- Any additional information required to reanalyze the data reported in this paper is available from the lead contact upon request.

EXPERIMENTAL MODEL AND STUDY PARTICIPANT DETAILS

Animals

Eight-week-old male C57/BL6J mice were purchased from the Model Animal Research Center of Nanjing University (Nanjing, China). The mice were housed in temperature- and humidity-controlled specific-pathogen-free (SPF) conditions, with access to adequate food and water supplies and a 12/12 h light-dark cycle. All procedures were approved by the Animal Care and Use Committee of Nanjing University and conducted in compliance with all relevant ethical rules.

Cell culture

Primary cortical neurons were obtained from E15-17 embryos of C57/BL6J mice. Briefly, after being seeded on poly-D-lysine-coated plates, the isolated cortical neurons were cultured in neurobasal media supplemented with GlutaMAX and B27. The subsequent experiments were conducted on the 7th to 8th day of culture.

Primary microglial cells were obtained from the cerebral cortex of 1- to 2-day-old C57BL/6J mice as previously described.[63] In brief, after digestion, centrifugation and filtering, glial cells were obtained, seeded into 75 cm² flasks and cultured in DMEM with FBS and penicillin−streptomycin for 14 days. Flasks were shaken gently, and microglial cells were collected and reseeded on the indicated plates for subsequent study.

METHOD DETAILS

Drugs

QHRD106 injection (purity: 98.73%, standard: 0.8 mL: 2000 IU) was provided by Changzhou Qianhong Biopharma Co., Ltd. (Jiangsu, China). QHRD106 was diluted with saline, given by intramuscular injection 2 h after the establishment of the MCAO model, and administered again three days after MCAO. HOE-140 (a B2R antagonist) and geldanamycin (GA, an HSP90AA1 inhibitor) were purchased from MedChemExpress (NJ, USA), and HOE-140 was subcutaneously administered twice daily in mice in a volume of 0.3 mg/kg body weight. R-715 (a B1R antagonist) was purchased from Tocris Bioscience (Bristol, UK) and was intraperitoneally administered daily in mice with a volume of 1 mg/kg body weight. LPS derived from *E. coli* 055:B5 was purchased from Sigma−Aldrich (St. Louis, USA). The sham group and MCAO model group received the same volume of saline.

Focal cerebral ischemia and LSCI

Mice were randomly subdivided into sham, saline, QHRD106-100 IU/kg, QHRD106-200 IU/kg, QHRD106-400 IU/kg, QHRD106(400 IU/kg) + HOE-140 and QHRD106(400 IU/kg) + R-715 groups. MCAO was used to establish a transient focal cerebral ischemia model in all mice except the sham operation group. In brief, mice were deeply anesthetized with 1% pentobarbital sodium (45 mg/kg i.p.). Next, a 6/0 monofilament nylon suture (Doccol Corporation, MA, USA) was inserted via the internal carotid artery into the beginning of the middle cerebral artery until a steep drop in regional cerebral flow was observed by laser Doppler flowmetry (Perimed Corporation, Stockholm, Sweden). After 1 h of ischemia, the suture was removed to achieve reperfusion, and the mice were injected with QHRD106, HOE-140, R-715 or saline. Sham-operated mice underwent the same procedures except for insertion of the suture. During surgery, the body temperature of the mice was maintained at $37 \pm 0.5°C$ with a heating pad.

In addition, LSCI was used to visualize the preoperative, perioperative and postoperative CBF. Using a laser (Perimed Corporation) directed at the skull, CBF images at different stages were collected for further analysis.

Behavioral testing

The neurological deficits of MCAO mice were evaluated by the rotarod test, forepaw grip strength measurement and mNSS assessment at 1, 3 and 7 days after MCAO. The mNSS was used to evaluate sensory function, motor function, reflexes and balance deficits in MCAO mice on a scale from 0 to 18. Higher scores indicated more severe deficits. Forepaw grip strength was measured with a grip strength meter (GS3, Bioseb, France). Each mouse was tested 5 times and the maximum strength value was recorded. For the rotarod test, the mice were pretrained for 3 days on rotarods (RWD Life Science, Shenzhen, China) before the MCAO procedure. In the formal test, the time the mice remained on the rotarod was recorded while the rotation speed of the rotarod was increased linearly, with a maximum time of 300 s and a maximum rotarod speed of 40 rpm.

OGD/R treatment

OGD/R was performed on primary cortical neurons to mimic ischemia *in vitro*. The cells were cultured in serum/glucose-free medium and then transferred into a hypoxia chamber (BillupsRothenberg, Del Mar, CA, USA) that contained 5% CO_2 and 95% N_2 for 35 min at 37°C. Then, the cells were returned to a normal incubator with normal medium for another 9 h.

Cell viability assay

A CCK-8 assay (Dojindo Molecular Technologies) was used to assess the viability of primary cortical neurons. Neurons were evenly plated on 96-well plates and treated with various concentrations of QHRD106. After OGD/R, 10 μL of CCK-8 reagent was added, and the plates were incubated at 37°C for 9 h. Finally, absorbance was measured at 450 nm with a microplate reader.

RNA isolation and quantitative real-time PCR

Total RNA was extracted from cerebral ischemic penumbra tissues using TRIzol reagent (Invitrogen, Frederick, MD, USA) according to the manufacturer's instructions. Then, RNA was reverse-transcribed into cDNA using a PrimeScript Reagent Kit (Vazyme, Nanjing, China). Quantitative real-time PCR was implemented on an ABI StepOne Plus PCR instrument (Applied Biosystems, CA, USA) with an SYBR green kit

(Applied Biosystems). The relative gene expression levels were quantified and normalized to GAPDH. The primer sequences used were as follows:

Nos2: F: CAGCTGGGCTGTACAAACCTT and R: CATTGGAAGTGAAGCGTTTCG.

Il6: F:GCTGGTGACAACCACGGCCT and R: AGCCTCCGACTTGTGAAGTGGT;

Tnfa: F: CAAGGGACAAGGCTGCCCCG and R: GCAGGGGCTCTTGACGGCAG;

Ccl2:F: TTGAGGTGGTTGTGGAAAAGG and R: GTGCTGACCCCAAGAAGGAAT;

Il1b:F: AAGCCTCGTGCTGTCGGACC and R: TGAGGCCCAAGGCCACAGG;

Il10: F: GGTTGCCAAGCCTTATCGGA and R: ACCTGCTCCACTGCCTTGCT;

Gapdh: F: GCCAAGGCTGTGGGCAAGGT and R: TCTCCAGGCGGCACGTCAGA.

Staining

TTC staining was used to measure the infarct volume of mice after MCAO. Brain tissues were continuously sliced into six sections (2-mm thick) and then dipped in 2% 2,3,5-triphenyltetrazolium chloride (TTC, Sigma–Aldrich) at 37°C for 15 min. The slices were photographed and analyzed with ImageJ software (ImageJ 1.5, NIH, USA). To correct for edema, the infarction volume was calculated as (contralateral hemisphere area – non-infarcted ipsilateral hemisphere area)/(2× contralateral hemisphere area)× 100%.

Apoptotic cells were detected using a TUNEL kit (Vazyme Biotech Co., Nanjing, China) according to the manufacturer's instructions. Briefly, 72 h after the MCAO operation, the mice were transcardially perfused with 0.9% saline and 4% paraformaldehyde (PFA) sufficiently under deep anesthesia. The brain was collected, fixed with 4% PFA and dehydrated with sucrose. After freezing, the brains were sliced into 20 μm sections for subsequent experiments. After permeabilization, the slices were incubated at room temperature for 2 h with TUNEL reagent. The TUNEL-labeled cells were observed under a fluorescence microscope (Olympus BX51, Japan) after DAPI staining.

For immunofluorescence staining, the brain sections were fixed with 4% paraformaldehyde, permeabilized with 0.2% Triton X-100 and blocked with 2% BSA. After incubation with the indicated primary antibodies against HMGB1 (Abcam, ab18256), NeuN (Abcam, ab104224) and Iba-1 (Abcam, ab5076) overnight at 4°C, the brain sections were incubated with the appropriate secondary antibodies, and DAPI was used to stain the cell nuclei. Images were captured using a confocal laser-scanning microscope (Olympus FV3000, Japan). Skeleton analysis was used to quantify microglial morphology in immunofluorescence staining images *in vivo*.[64]

Working reagents for dual labeling with calcein-AM and PI dual labeling (Dojindo Molecular Technologies, Tokyo, Japan) were prepared according to the manufacturer's instructions. After being washed with PBS, primary cortical neurons in different groups were incubated with the working reagents for 15 min in a dark incubator. After being washed, the neurons were observed by a fluorescence microscope. The calcein-AM-labeled neurons, which showed green fluorescence, were alive, while the PI-labeled neurons, which showed red fluorescence, were apoptotic.

For silver staining, a Pierce Silver Stain Kit (Thermo Fisher Scientific) was used to detect protein in polyacrylamide gels rapidly with high sensitivity according to the manufacturer's instructions. In brief, after fixing and washing, the polyacrylamide gels with separated proteins were incubated with Sensitizer Working Solution, Stain Working Solution and Developer Working Solution in sequence. Once the desired band intensity was reached, the Developer Working Solution was replaced with Stop Solution.

PLA

PLA was performed using a Duolink *In Situ* Kit (Sigma–Aldrich) according to the manufacturer's instructions. Briefly, after being blocked, brains and cells were treated with anti-HSP90AA1 (Proteintech, 60318-1-lg) and anti-HMGB1 (Abcam, ab18256) antibodies overnight. After being washed, the samples were

incubated with PLA probes and ligation solution. The samples were incubated in polymerase solution to amplify the signal. Fluorescence was observed using a confocal laser-scanning microscope after staining with DAPI.

ELISA

Blood samples were collected from the orbital veins of anesthetized mice into sterile Eppendorf tubes, then refrigerated at 4°C for 2 h. Following centrifugation for 10 min at 3000 rpm, the supernatant serum was collected for subsequent study. The levels of HMGB1 in mouse serum were measured with an HMGB1 ELISA kit (Cusabio Biotech, Wuhan, China) according to the manufacturer's instructions. The absorbance was measured with a microplate reader (Tecan Trading AG, Switzerland).

Western blot analysis

RIPA buffer containing phosphatase and protease inhibitors was used to extract proteins from samples. The concentration of protein was measured with a BCA kit (Thermo Fisher Scientific, Rockford, IL, USA). The proteins were separated by SDS−PAGE and then transferred onto PVDF membranes. After being blocked, the membranes were incubated with primary antibodies against Bax (Bioworld, Minneapoils, MN, USA, BS2538), Bcl-2 (Bioworld, BS1511), iNOS (BD Biosciences, NJ, USA, 610328), MCP-1 (Proteintech, Wuhan, China, 66272-1-Ig), TNF-α (Proteintech, 17590-1-AP), β-actin (Bioworld, AP0060), lamin B1 (Bioworld, AP6001), HMGB1 (Abcam, Cambridge, MA, USA, ab18256), GAPDH (Bioworld, AP0063), acetyl-lysine (PTM-BioLab, Hangzhou, China, PTM-105) and HSP90AA1 (Invitrogen, PA3-013) overnight at 4°C. Next, after the membranes were incubated with HRP-conjugated secondary antibodies and washed with TBST, the bands were visualized by a GelPro system (Tanon Technologies, Shanghai, China) using an ECL Detection Kit (Millipore, Billerica, MA, USA), and the band intensities were analyzed by ImageJ software.

Proteomics analysis

Total proteins were extracted from the cerebral ischemic penumbra tissues of different groups three days after MCAO. Proteomics analysis was conducted by OE Biotech Co., Ltd. (Shanghai, China). Hierarchical cluster analysis of DEPs was used to identify the differentially expressed proteins in different groups. KEGG pathway analysis and GO analysis were used to further analyze the DEPs.

Coimmunoprecipitation

The protein lysates were incubated with 1 μg of HMGB1 antibody (Abcam, ab18256) overnight at 4°C. Subsequently, a 30 μL volume of Protein A/G PLUS-agarose beads (Millipore) was added for another 3 h. After being centrifuged and washed with lysis buffer three times, the beads were combined with 30 μL of 2× loading buffer and boiled for 5 min. The degree of acetylation of HMGB1 and the binding levels of HSP90AA1 were analyzed by western blotting using antibodies against acetyl-lysine (PTM-BioLab, PTM-105) and HSP90AA1 (Invitrogen, PA3-013). Protein lysates were used as positive controls for western blot analysis without immunoprecipitation.

Cytoplasmic and nuclear protein extraction

Extraction was performed with an NE-PER Nuclear Cytoplasmic Extraction Reagent kit (Thermo Fisher Scientific) according to the manufacturer's instructions. Briefly, fresh tissues or primary microglial cells in different groups were washed with cold PBS and then collected in cold tubes. The cells were resuspended, and the tissues were homogenized in cytoplasmic extraction reagent I. After vortexing for 15 s and incubation on ice for 10 min, cytoplasmic extraction reagent II was added to the suspension. Following vortexing for 5 s, incubation on ice for 1 min and centrifugation for 5 min at 16 000 × g, the supernatant was collected as the cytoplasmic extract, and the insoluble pellet fraction was resuspended in nuclear extraction reagent. After vortexing and repeated incubation on ice, the nuclear components were extracted after a final centrifugation. Cytoplasmic extraction and nuclear extraction were used for subsequent western blot analysis.

Determination of extracellular HMGB1 levels

Extracellular HMGB1 levels were measured in the same amount of culture medium from equal numbers of microglia or neurons in each group. Before stimulation, the normal medium was replaced with serum-free medium. After stimulation for the indicated durations, the medium was collected into a tube, and 250 μL of chloroform and 1 mL of methanol were added to each 1 mL of medium. Following centrifugation at

16 000 ✕ g for 5 min, the supernatant was discarded. Then, the precipitate was washed with 1 mL methanol, centrifuged at 16 000 ✕ g for 5 min and dried. After being resuspended in 1✕ loading buffer and boiled at 100°C for 5 min, the samples were subjected to western blot analysis.

QUANTIFICATION AND STATISTICAL ANALYSIS

For quantification of the immunofluorescence images, three fields of each sample were used for quantification, and then the values were averaged to obtain one value for each sample. Generally, there were three samples in each statistical analysis.

Statistical analysis

Data were analyzed by GraphPad Prism 8.0 Software and shown as the means $\pm$ standard error of the mean (SEM). One-way or two-way ANOVA followed by Tukey's post hoc test was used for data that passed the Shapiro−Wilk normality test and the Brown-Forsythe test of homogeneity of variances for multiple-group comparisons. $p < 0.05$ was considered statistically significant.